Effect of Mg^{2+} concentration on Ca^{2+} uptake kinetics and structure of the sarcoplasmic reticulum membrane

Francisco J. Asturias and J. Kent Blasie
Department of Chemistry, University of Pennsylvania, Philadelphia, Pennsylvania 19104

ABSTRACT Direct measurements of phosphorylation of the Ca^{2+}ATPase of the sarcoplasmic reticulum (SR) have shown that the lifetime of the first phosphorylated intermediate in the Ca^{2+} transport cycle, E_1~P, increases with decreasing [Mg^{2+}] (Dupont, Y. 1980. *Eur. J. Biochem.* 109:231–238). Previous x-ray diffraction work (Pascolini, D., and J.K. Blasie. 1988. *Biophys. J.* 54:669–678) under high [Mg^{2+}] conditions (25 mM) indicated that changes in the profile structure of the SR membrane could be responsible for the low-temperature transient trapping of E_1~P that occurs at temperatures below 2–3°C, the upper characteristic temperature t_h for lipid lateral phase separation in the membrane. We now present results of our study of the Ca^{2+} uptake kinetics and of the structure of the SR membrane at low [Mg^{2+}] ($\leq$100 μM). Our results show a slowing in the kinetics of both phases of the Ca^{2+} uptake process and an increase in the duration of the plateau of the fast phase before the onset of the slow phase, indicating an increase in the lifetime (transient trapping) of E_1~P. Calcium uptake kinetics at low [Mg^{2+}] and moderately low temperature (~0°C) are similar to those observed at much lower temperatures (~ – 10°C) at high [Mg^{2+}]. The temperature-induced structural changes that we observed at low [Mg^{2+}] are much more pronounced than those found to occur at higher [Mg^{2+}]. Also, at the lower [Mg^{2+}] the upper characteristic temperature t_h for lipid lateral phase separation was found to be higher, at ~8–10°C. Our studies indicate that both temperature and [Mg^{2+}] affect the structure and the functionality (as measured by changes in the kinetics of Ca^{2+} uptake) of the SR membrane. Membrane lipid phase behavior and changes in the Ca^{2+}ATPase profile structure seem to be related, and we have found that structural changes are responsible for the slowing of the kinetics of the fast phase of Ca^{2+} uptake, and could also mediate the effect that [Mg^{2+}] has on E_1~P lifetime.

INTRODUCTION

The effect of temperature and Mg^{2+} concentration on the kinetics of Ca^{2+} uptake by isolated sarcoplasmic reticulum (SR) vesicles has been extensively studied (1–4). Previous work in our laboratory established a relation between the temperature dependence of Ca^{2+} uptake by SR vesicles and variations in the electron density profile structure of the membrane (5). It was found, for the higher Mg^{2+} concentration studied (~25 mM), that a temperature-driven reversible structural transition occurs in the membrane profile with decreasing temperature at 2–3°C. That transition appeared to be linked to the transient trapping of the Ca^{2+}ATPase in the E_1~P conformation, the first phosphorylated intermediate in the Ca^{2+} uptake cycle (6), and therefore it was proposed that at such "high" [Mg^{2+}], the transient trapping of the Ca^{2+}ATPase in the E_1~P conformation for temperatures below 2–3°C could be a phenomenon of structural origin. On the other hand, it has been proposed that the effect on Ca^{2+} uptake kinetics and lifetime of the E_1~P intermediate observed at lower [Mg^{2+}] are due to differences in the substrate available to the enzyme (7). According to this view, the formation of different phosphorylated enzyme intermediates, depending on whether the ATPase utilizes Ca^{2+} · ATP or Mg^{2+} · ATP as its substrate, is directly responsible for the changes in the kinetics of Ca^{2+} uptake. As this explanation was fundamentally different from that proposed to explain the observed behavior of the SR membrane system at higher Mg^{2+} concentrations, we decided to investigate what influence, if any, structural changes could have on the functionality of the SR system at low [Mg^{2+}].

An equally important reason to study the Ca^{2+} uptake kinetics and the structure of the SR membrane at lower Mg^{2+} concentrations was that it has been reported that the lifetime of the E_1~P intermediate increases dramatically with decreasing Mg^{2+} concentration and x-ray diffraction studies of the structure of the E_1~P intermediate would be greatly facilitated if the lifetime of the intermediate could be prolonged without destroying the functionality of the Ca^{2+}ATPase.

In this paper we report the results of our study of the kinetics of Ca^{2+} uptake and of the profile and in-plane structure of the SR membrane as a function of temperature and Mg^{2+} concentration.

0006-3495/89/04/739/15 $2.00

METHODS

Dispersions of SR vesicles were prepared from albino rabbit hind leg muscle. The SR preparation was purified using a zonal density gradient centrifugation technique, as previously described (8). The Ca^{2+}ATPase accounts for at least 90% of the protein present in the purified SR vesicles. No Mg^{2+} salts were used during the isolation and purification of the vesicles, therefore all Mg^{2+} present was that which came from the starting muscle material. The total Mg^{2+} concentration in the final preparation was spectrophotometrically determined to be <40 μM.

Ca^{2+} uptake by SR vesicular dispersions and by partially dehydrated multilayers of SR vesicles was studied using a time-sharing double-beam spectrophotometer system (Johnson Research Foundation, University of Pennsylvania) to follow changes in the absorbance of the Ca^{2+}-sensitive metallochromic indicator Arsenazo (III). Calcium uptake was initiated via photolysis of a caged-ATP compound. A more detailed description of the method has been presented previously (9, 10). The kinetics of Ca^{2+} uptake were studied as a function of both temperature between 2 and 15°C, and [Mg^{2+}] between 25 mM (8 mM for dispersions) and 100 μM (40 μM for dispersions).

For the x-ray diffraction experiments, multilayers of purified SR vesicles were prepared by centrifugation of a suspension of SR vesicles in a special sedimentation cell onto aluminum foil strips as described previously (11). The multilayers were mounted on special supports designed to make possible the recording of both lamellar diffraction (x-ray beam at grazing incidence with respect to the surface of the cylindrically curved multilayer), and equatorial diffraction (x-ray beam at normal incidence to the surface of the multilayer) from the same multilayer.

After being mounted, a sample was partially dehydrated at 7°C for an average of 36 h over a saturated KCl solution (relative humidity, 88%). For the x-ray experiment the partially dehydrated multilayer was transfered to a sealed cannister where the relative humidity was again held constant at 88%. During the x-ray experiment the cannister was kept in a temperature-controlled specimen chamber whose temperature had been set to 15°C. The sample was then allowed to equilibrate for 60–90 min. To study the effect of temperature on the lamellar diffraction the following procedure was used. After recording lamellar and equatorial diffraction from the sample at 15°C the temperature was slowly lowered to a new desired value, the sample was allowed to equilibrate for a short period of time, and both diffraction patterns at the new temperature were recorded. The process was repeated until the temperature of the sample reached 2°C. The temperature was usually changed by 3° steps each time, and it was lowered at a rate of ~0.05°C/min. The samples seemed to be able to follow the temperature change closely. Once the desired temperature was reached, no further changes in the diffraction were observed if the sample was left at that temperature for times of up to 3–4 h. Exposure times were 300 s for both the lamellar and the equatorial patterns, and the diffraction was recorded with a two-dimensional, position-sensitive detector (Nicolet Instruments Co., Madison, WI) interfaced to a dedicated computer (Cadmus Computer Systems, Inc., Lowell, MA). A GX-13 rotating anode x-ray generator (Marconi Avionics, Ltd., Borenhamwood, UK) was used to produce an x-ray beam that was line-focused at the detector via Franks optics (12) with a 20-cm-long Ni-coated quartz mirror. For the equatorial diffraction experiments, the line-focused x-ray beam height was cut down using slits until the direct beam, as seen by the detector, was a point with size limited by the detector's resolution (~800 μm square). Specimen to detector distances (through He-filled flight tubes) were 65 cm for the lamellar diffraction experiments, and 9 cm for the equatorial diffraction experiments. All two-dimensional diffraction patterns were run through a correction algorithm that employs a pattern obtained by uniformly illuminating the detector with an ^{55}Fe source, to correct for nonuniformities in the detector's sensitivity. After correction, the patterns were stored and integrated to produce one-dimensional patterns used for analysis. In the case of the lamellar diffraction patterns an angular integration algorithm was used to integrate the intensity of the arc-shaped reflections over the multilayer mosaic spread of ±15°. The integrated one-dimensional lamellar intensity functions $I_0(r^* - 0, z^*)$, where r^* and z^* are reciprocal space coordinates, were corrected for lamellar background scattering by subtracting a piecewise continuous exponential approximation to the background scattering (5). Finally, a Lorentz correction (13) of z^* was applied (allowing for the cylindrical curvature of the specimen), to provide $I_c(r^* - 0, z^*)$. In the case of the two-dimensional equatorial diffraction patterns a background pattern was collected using the same experimental set-up, but with no sample present, and a pixel-by-pixel background subtraction was done. The ringlike patterns were then angularly integrated over 360° to obtain a one-dimensional intensity function $I(r^*, z^* - 0)$. All data analysis was done on a VAX 11-750 computer (Digital Equipment Corp., Westboro, MA).

RESULTS

Ca^{2+} uptake as a function of temperature and [Mg^{2+}]

Calcium uptake was studied as a function of temperature and [Mg^{2+}] for both vesicular dispersions and partially dehydrated oriented multilayers of SR vesicles. Previous work in our laboratory (10) demonstrated that the partially dehydrated multilayers used for the x-ray diffraction experiments and SR vesicular dispersions are very nearly equivalent with respect to their Ca^{2+} uptake behavior, and therefore the use of dispersions or multilayers is determined mostly by convenience. All Ca^{2+} uptake measurements were done using an SR preparation with a total protein content of 67% (14). This preparation has Ca^{2+} uptake rates that, when expressed in terms of the total amount of enzyme that can be phosphorylated, are identical to those of the more purified preparation used for the x-ray diffraction experiments (15). The need to perform several different control experiments, as well as repeated runs to check reproducibility made it more convenient to use the lower protein content preparation, that also remains viable for longer periods of time under the conditions necessary for the Ca^{2+} uptake experiments.

The uptake of Ca^{2+} by SR is well characterized. It has been shown to be at least a biphasic process, with an initial fast phase that has been associated with occlusion of Ca^{2+} and formation of the first phosphorylated intermediate E_1~P. This is followed by a slow phase associated with enzyme turnover and translocation of Ca^{2+} across the membrane. Calcium uptake is progressively slowed by decreasing temperature, and at low temperatures the fast phase is followed by a "plateau" that precedes the onset of the slow phase. This plateau after the fast phase has been associated with transient trapping of the Ca^{2+}ATPase in

the E_1~P conformation. For high Mg^{2+} concentrations (~10–25 mM) and temperatures of −2–0°C, the enzyme can be transiently trapped in the E_1~P conformation for 6–8 s as judged by the duration of the plateau after the fast phase. To study the effect of Mg^{2+} concentration, we measured Ca^{2+} uptake under a set of different temperature and $[Mg^{2+}]$ conditions. Typical Ca^{2+} uptake curves are presented in Fig. 1, and the results obtained can be summarized as follows. At any temperature in the range studied (−2–25°C) a decrease in the Mg^{2+} concentration greatly reduces the rate of Ca^{2+} uptake. Fig. 1A shows Ca^{2+} uptake curves for SR vesicular dispersions at 15°C for ~8 mM and ~40μM $[Mg^{2+}]$. At this temperature, the initial fast phase is not resolved in the time scale of the figure. The changes observed (more rapid and greater Ca^{2+} accumulation) are the result of faster overall turnover rate of the enzyme at the higher $[Mg^{2+}]$. Fig 1, *B* and *C*, illustrate what is observed at lower temperatures. Fig. 1 *B* shows typical uptake curves for SR multilayers at −2°C and 25 mM $[Mg^{2+}]$. The initial fast phase only

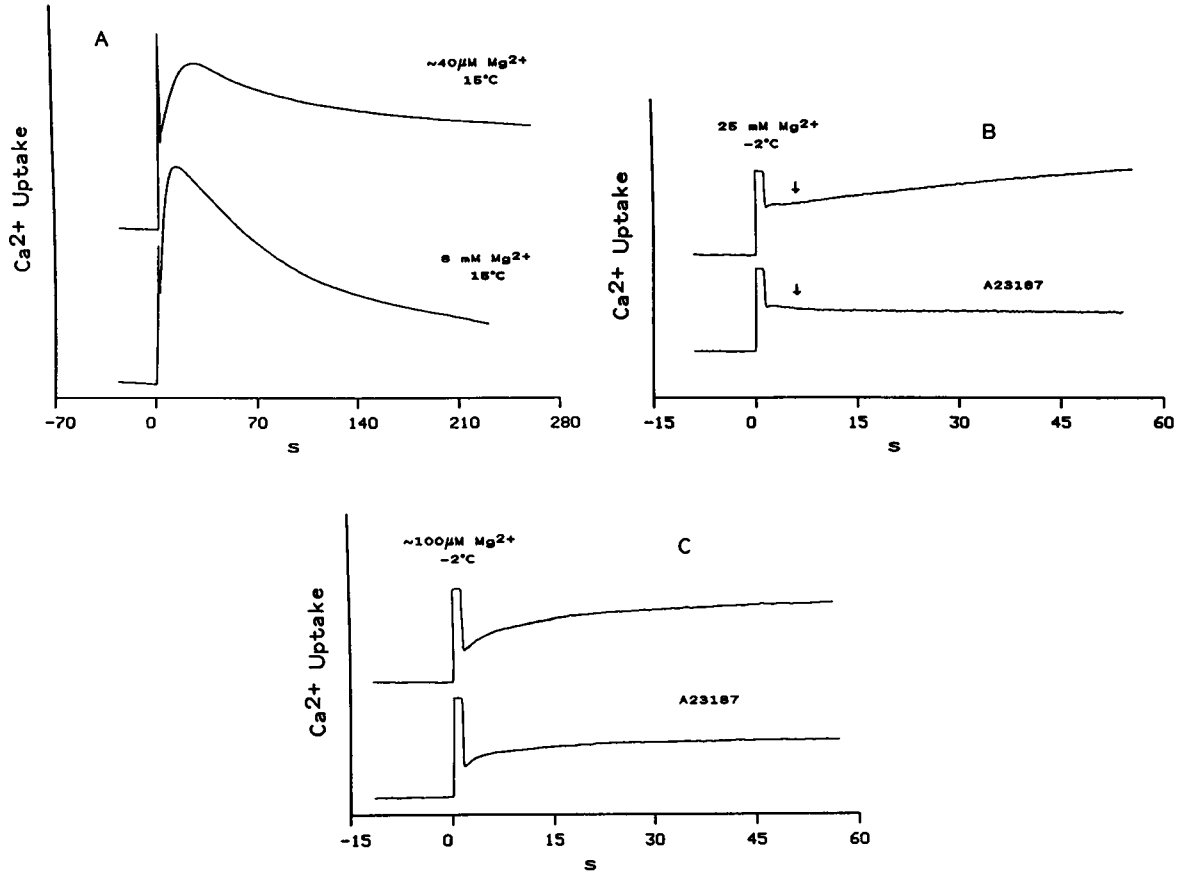

FIGURE 1 Typical Ca^{2+} uptake kinetics for SR vesicular dispersions and oriented multilayers at different temperatures and $[Mg^{2+}]$. The absorbance of the Ca^{2+}-sensitive metallochromic indicator Arsenazo (III) at 660 vs. 690 nm (which changes linearly with $[Ca^{2+}]$ in the concentration range studied) is plotted as a function of time. For these experiments, Ca^{2+} uptake was initiated by flash photolysis of caged ATP using a 200-W mercury-arc lamp (800 ms flash), and changes in absorbance were followed using a spectrophotometer system and recorded using a chart recorder. The SR vesicular dispersions contained 40 mM Tris maleate, 120 mM KCl, 100 μM Arsenazo III, 1 mg SR protein/ml, 1 mM caged ATP, 50 μM Ca^{2+} in addition to the Ca^{2+} provided by the SR vesicles, and the indicated $[Mg^{2+}]$. The SR multilayers were prepared sedimenting 1 mg SR protein, and contained ~100 mM Tris maleate, 300 mM KCl, 125 μM Arsenazo III, 4 mM glutathione, 65 μM Ca^{2+} in addition to the Ca^{2+} provided by the SR, and the indicated $[Mg^{2+}]$. (*A*) Ca^{2+} uptake (SR vesicular dispersions) at 15°C for $[Mg^{2+}]$ ~8 mM and ~40 μM. See text for more details. (*B*) Ca^{2+} uptake (SR multilayers) at −2°C and ~25 mM $[Mg^{2+}]$ in the presence and in the absence of Ca^{2+} ionophore A23187. The initial rise of the fast phase is not resolved in either of these two Ca^{2+} uptake curves, and the plateau after the fast phase (indicating transient trapping of the E_1~P intermediate) before the onset of the slow phase can be observed to last for ~6 s. See text for more details. (*C*) Ca^{2+} uptake (SR multilayers) at −2°C and ~100 μM $[Mg^{2+}]$ in the presence and in the absence of Ca^{2+} ionophore A23187. The rise of the fast phase is now resolved (note that the curve extrapolates to the initial concentration at time zero). The fast phase is followed by a long plateau (~60 s) of nearly constant $[Ca^{2+}]$, indicating trapping of the Ca^{2+}ATPase in the E_1~P conformation. This is eventually followed by the slow phase, whose rate is greatly diminished under these conditions. The ionophore experiments confirm that the Ca^{2+} uptake observed is in fact due mostly to the initial fast phase. See text for more details.

lasts for ~2 s and cannot be seen in the figure (it is obscured by an experimental artifact seen as the square-shaped pulse), but the plateau that follows it can be observed to last for ~6 s (the end of the plateau is approximately indicated by the arrows). The ionophore-sensitive slow phase can also be observed under these conditions, as evidenced by the difference between the upper (no ionophore) and the lower (ionophore) curves. Finally, the Ca^{2+} uptake curves presented in Fig. 1 *C* correspond to the same conditions as those in Fig. 1 *B*, except that the $[Mg^{2+}]$ is much lower (~100 μM). The decrease in $[Mg^{2+}]$ slows the ionophore-insensitive fast phase, and greatly increases the duration of the plateau that follows it. This is evidenced by the fact that both curves (with and without ionophore) are very similar. The fast phase (that lasts for several seconds under these conditions) is resolved, and the plateau is observed to last for ~60 s. The slow phase can still be observed, but is not shown in the figure.

The effect of Mg^{2+} concentration is very significant. Decreasing the concentration of Mg^{2+} by an order of magnitude at constant temperature has an effect that is roughly comparable with that of decreasing the temperature by 10°C at constant $[Mg^{2+}]$. Measurement of the duration of the plateau after the fast phase for temperatures of −2–0°C indicate that the Ca^{2+}ATPase can be transiently trapped in the E_1~P conformation for times of up to 60 s at low $[Mg^{2+}]$ (~40–100 μM), and that this plateau is followed nevertheless by a very slow "slow phase", i.e., enzyme turnover can still be detected.

Equatorial diffraction as a function of temperature

The equatorial diffraction intensity $I(r^*, \phi^*, z = 0)$, for r^*~4–5 Å^{-1}, arises from the packing of lipid fatty-acid chains in mosaic domains in the membrane plane, and it therefore consists of a circularly symmetric intensity distribution, namely a ring with mean radius and width determined in turn by the average chain-to-chain spacing and by the distribution of that spacing with respect to its mean value. Melted, disordered chains will give rise to a diffuse ring, whereas a more ordered arrangement of frozen chains in a lattice will give rise to a sharp ring with larger mean radius.

For a given sample and temperature, both lamellar and equatorial diffraction patterns were recorded. This procedure made it possible to directly correlate, as a function of temperature, changes observed in the lamellar diffraction with changes observed in the equatorial diffraction. As mentioned before, the two-dimensional equatorial diffraction patterns $I(r^*, \phi^*, z^* = 0)$ were angularly integrated over ϕ^* to produce a one-dimensional function $I(r^*, z^* = 0)$ that represents the radial dependence of the diffracted intensity arising from the lipid chain packing in the membrane plane. Such integrated equatorial diffraction patterns as a function of temperature for $[Mg^{2+}]$ ~100 μM are presented in Fig. 2. It can be seen that at high temperatures (>10°C) only one broad, symmetric

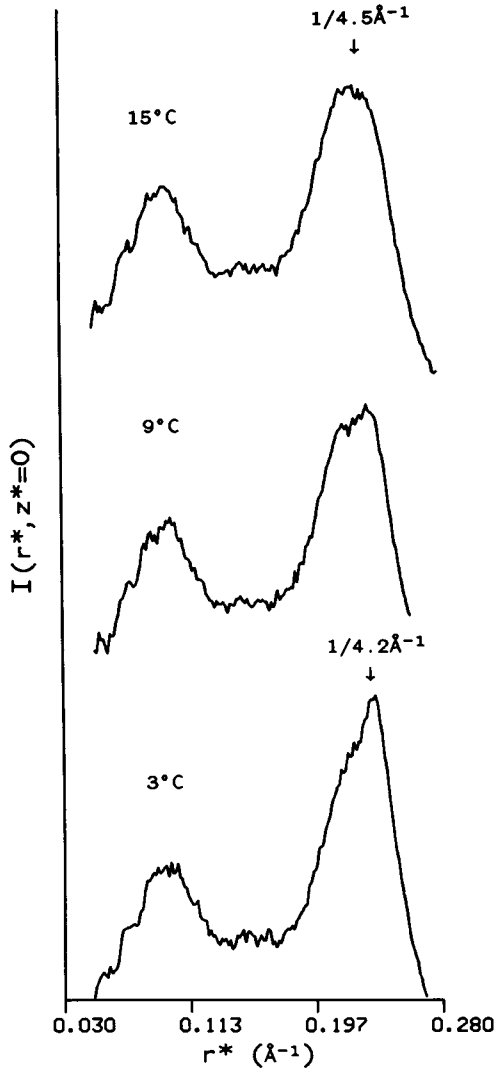

FIGURE 2 One-dimensional intensity functions $I(r^*, z^* = 0)$ obtained by angular integration of the SR equatorial diffraction patterns for partially dehydrated (88% relative humidity), oriented multilayers of flattened SR vesicles at low (~100 μM) $[Mg^{2+}]$. The broad symmetric peak (1/4.5 Å^{-1}) for temperatures above 8–10°C indicates a liquid-like distribution of melted lipid chains in the membrane plane. For temperatures below 8–10°C the peak becomes progressively more asymmetric with decreasing temperature. A sharper peak (1/4.2 Å^{-1}) characteristic of crystalline domains of frozen lipid chains first appears when the temperature is decreased to 8–10°C. This is evidence of lipid lateral phase separation in the membrane.

diffraction peak corresponding to a mean Bragg spacing of ~1/4.5 $Å^{-1}$ can be observed. As the temperature is decreased the broad peak becomes asymmetric, and a sharp component starts to appear on the high-angle side of the original peak. This sharp reflection corresponds to a mean Bragg spacing of ~1/4.2 $Å^{-1}$, and its intensity increases as the temperature is lowered. Analysis of these equatorial diffraction patterns obtained from different samples indicates that the sharp component at ~1/4.2 $Å^{-1}$ always appears only when the temperature drops below ~10°C. The additional diffuse maxima in the low-angle region of the patterns corresponds to a mean Bragg spacing of ~1/10 $Å^{-1}$ and arises from the α-helices in the protein (16). The shape and intensity of this peak seems to remain fairly constant over the temperature range studied (3–15°C).

Lamellar diffraction as a function of temperature

The lamellar diffraction patterns $I(r^* = 0, z^*)$ obtained from the multilayer specimens consist of a few discrete orders of diffraction in the region of lower z^*, indexed as l/d, for l an integer and d the multilayer lattice periodicity. For higher values of z^* the significant amount of disorder in the multilayer lattice samples causes the diffraction to consist of continuously varying intensity, with maxima and minima arising from the unsampled structure factor modulus squared for the membrane-pair profile. Diffraction was recorded up to $z^*_{max} \simeq 0.080$ $Å^{-1}$, which corresponds to a spatial resolution of ~13 Å in the membrane-pair profile.

All the lamellar diffraction maxima are arc-shaped, due to mosaic spread of ~ ±15° in the multilayer samples. Uncorrected, one-dimensional intensity functions $I_0(r^* = 0, z^*)$, obtained by angular integration of two-dimensional lamellar diffraction patterns over the multilayer mosaic spread are shown in Fig. 3 for several temperatures and $[Mg^{2+}]$ ~100 μM. It is important to notice the variation in the intensity of the different diffraction maxima, most significantly in the case of the third and fourth diffraction orders, and the three maxima in the region of 0.045 $Å^{-1} \leq z^* \leq$ 0.075 $Å^{-1}$. One convenient way to parametrize changes in the lamellar diffraction as a function of temperature is to plot the ratio of the peak intensities of the third to fourth orders as measured from the uncorrected diffraction patterns. This kind of plot is presented for four different samples in Fig. 4. The ratio of the intensities of the third and fourth orders changes continuously, but there is a well-defined temperature range where the rate at which that ratio varies with temperature changes significantly. For the present experiments that temperature corresponds (as

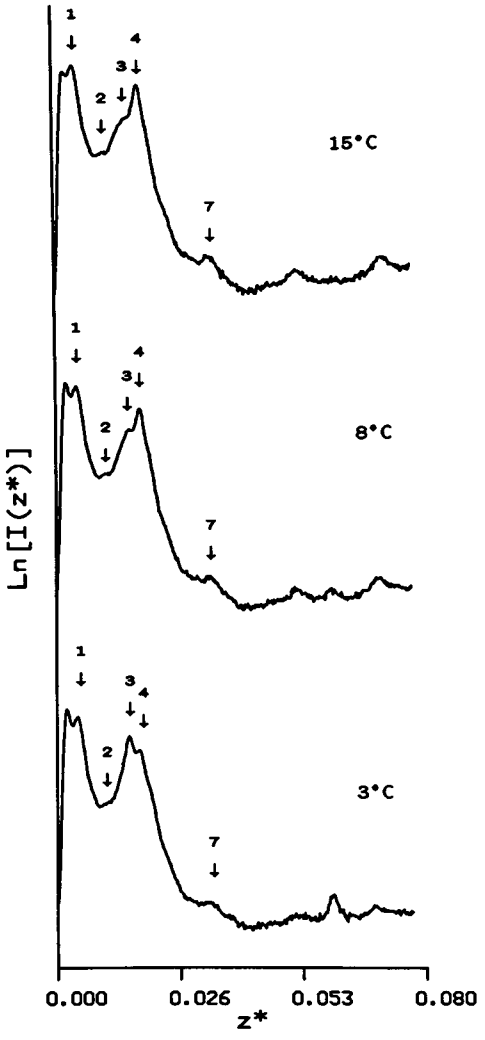

FIGURE 3 Semilogarithmic plots of lamellar diffraction $I_0(z^*)$ as a function of temperature for partially dehydrated (88% relative humidity), oriented multilayers of flattened SR vesicles at low (~100 μM) $[Mg^{2+}]$. The numbered arrows indicate the position of lamellar Bragg orders. Diffraction maxima at higher values of z^* arise from the unsampled unit cell structure factor. The relative intensity throughout the lamellar diffraction shows a temperature dependence, and the third and fourth orders undergo the most noticeable changes. All patterns represent a total collection time of 300 s.

can be seen from Fig. 3) to 8–10°C. This observation suggests that the multilayer unit cell profile structure (which contains the membrane-pair profile) undergoes a temperature-dependent structural "transition" at 8–10°C for $[Mg^{2+}]$ ~100 μM. For all samples examined, the changes in the lamellar diffraction induced by exposure to low temperature (~2°C) could be reversed in a short period of time (5–20 min) by reequilibration at higher temperature.

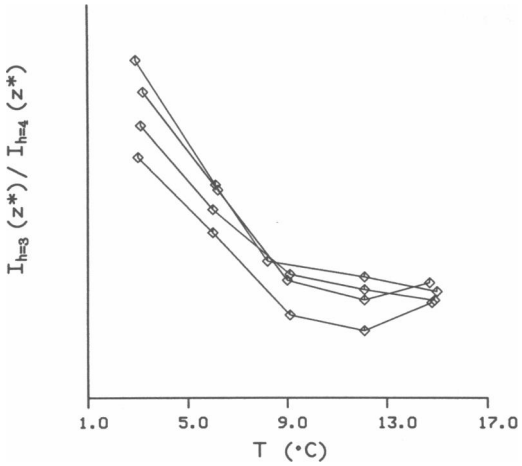

FIGURE 4 Ratio of the peak heights of the third to the fourth orders as measured from the uncorrected lamellar diffraction patterns $I_c(z^*)$ as a function of temperature. Data from four different samples are presented. For each sample the temperature was progressively changed. The different points in a particular curve represent the ratio of the intensities at the corresponding temperature. Note that the curves have two distinct regions of nearly linear behavior, and that there is a well-defined temperature (8–10°C) where the rate at which the ratio of the intensities varies with temperature changes.

SR membrane electron density profiles as a function of temperature

The lamellar diffraction patterns $I_c(r^* = 0, z^*)$, background scattering and Lorentz corrected as indicated, were analyzed using the Generalized Fourier Synthesis Deconvolution Method, GFSDM (17), which assumes a centrosymmetric structure for the multilayer unit cell profile. To check the phases obtained from the GFSDM analysis a box refinement algorithm (18) was also utilized. The electron density profiles for the multilayer unit cell (containing the two apposed SR membranes of the flattened vesicle) obtained from GFSDM were calculated to a resolution of 13 Å. The box refinement analysis was only carried out to a lesser resolution (35 Å), mostly to confirm the phases assigned by GFSDM to the first four lamellar diffraction orders, as allowed by the Fourier sampling theorem (19) given the fact that the lamellar diffraction maxima at large z^* are relatively weak. The phase combination obtained using GFSDM was confirmed by the box refinement analysis in all cases. The phases obtained for the different diffraction orders are presented in Table 1, along with those obtained for similar samples under high Mg^{2+} conditions (5). Note that in the case of the high $[Mg^{2+}]$ (25 mM) samples the phase of the first order changed in going through the transition temperature at 2–3°C. For samples with low $[Mg^{2+}]$ (~100 μM) the phase of the first order is constant in the temperature range examined, and reversed with respect to that observed at high Mg^{2+} concentrations and high temperature. The nature, extent, and temperature dependence (see Fig. 4) of the changes observed in the lamellar diffraction patterns were the same for all samples examined. All the lamellar diffraction patterns were analyzed as described above, and the electron density profiles obtained for different samples under the same experimental conditions were essentially identical. One of the samples of the set examined, was chosen as "typical" and electron density profiles obtained for that sample at 15 and 3°C are shown in Fig. 5. The electron density profiles

TABLE 1 Phases assigned to lamellar diffraction maxima as a function of temperature and $[Mg^{2+}]$

$[Mg^{2+}]$	Above t_h	Below t_h
100 μM (t_h ~ 9°C)	−+−−0−	−+−−+−
25 μM (t_h ~ 2°C)	++−−00	−+−−00

Lamellar diffraction patterns for 25 mM $[Mg^{2+}]$ were collected at lower resolution, and therefore less maxima had to be phased. In the case of the diffraction patterns for 100 μM $[Mg^{2+}]$ (see Fig. 3), the first region of constant phase includes the first diffraction order, the second region includes orders 2 to 5, and the third region includes orders 6 and 7. The additional three regions of constant phase correspond to the three maxima in the region 0.04 $Å^{-1} < z^* < 0.08$ $Å^{-1}$ (the second maxima only appearing at low temperature).

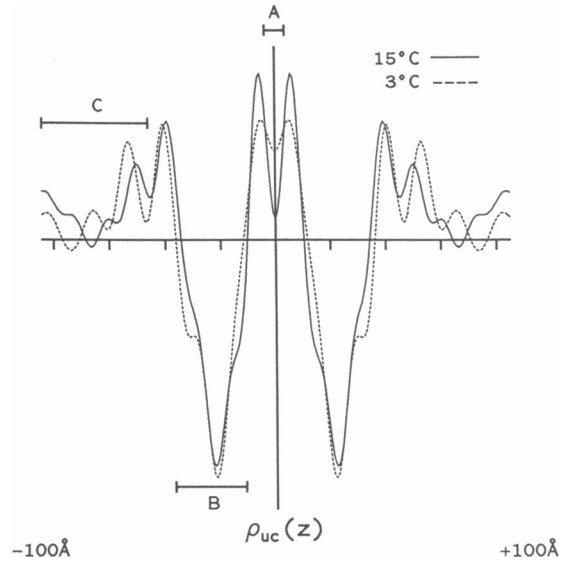

FIGURE 5 Electron density profiles for the SR membrane for $[Mg^{2+}]$ ~100 μM, calculated to a resolution of ~13 Å using a direct general Fourier synthesis deconvolution method of analysis. Note the changes induced by temperature, especially the change in the width of the intravesicular water space (*A*), an increase in the width of the hydrocarbon core region of the membrane (*B*), and changes in the electron density in the region at the extravesicular membrane surface (*C*).

corresponding to this typical sample were also used for the model calculations described in the Discussion section. Note that the changes induced by decreasing temperature include a change in the width of the intravesicular water space (A), an increase in the width of the hydrocarbon core region of the membrane (B) (the separation between the lipid polar head groups went from 42 Å at 15°C to 44 Å at 3°C), and changes in the electron density in the region of the extravesicular membrane surface (C) containing the "headpiece" of the Ca^{2+}ATPase, these regions of the membrane profile having been so identified previously (20). Examination of the calculated autocorrelation functions for the multilayer profile structures, and of the values obtained for the multilayer lattice disorder parameter provided by the GFSDM analysis indicates that the degree of lattice disorder in the samples increased as the temperature was decreased.

DISCUSSION

Ca^{2+} uptake kinetics as a function of temperature and $[Mg^{2+}]$

The results obtained from the Ca^{2+} uptake measurements at different Mg^{2+} concentrations indicate, in agreement with results reported by others (1–4), that the kinetic behavior of the Ca^{2+}ATPase is significantly affected by changes in $[Mg^{2+}]$. We observed a slowing down of both phases of Ca^{2+} uptake, as well as increased duration of the plateau after the initial fast phase. We interpret this latter effect as an indication of transient trapping of the Ca^{2+}ATPase in the E_1~P conformation. Our experiments therefore monitor the transient trapping of the enzyme in this conformation indirectly, and agree with previous studies which directly measured E_1~P lifetime using isotopic methods (1, 21). This result further confirms the identification of the plateau of the fast phase with transient trapping of the enzyme in the E_1~P conformation before the onset of the slow, Ca^{2+} translocation phase.

At high $[Mg^{2+}]$ ($\geq$8 mM) the Ca^{2+}ATPase can be transiently trapped in the E_1~P conformation for 8–10 s if the temperature is lowered to ~ -2°C. Transiently trapping the enzyme in such conformation for a longer time without rendering it nonfunctional would greatly facilitate the acquisition of information about the structure of the first phosphorylated intermediate. At high $[Mg^{2+}]$ that requires the use of even lower temperatures (~ -10°C) which make it necessary to use cryoprotective agents (Itshak, F., and J. K. Blasie, unpublished results). Our present results indicate that, as first reported by DuPont (1), at low $[Mg^{2+}]$ ($\leq$100 μM) $E_1 \sim P$ can be transiently trapped for a longer time (~60 s) at temperatures that do not require the use of cryoprotective agents (0–2°C). That the enzyme remains functional even at low temperature and at low $[Mg^{2+}]$ is evidenced by the fact that some very slow turnover (slow phase) can still be observed even under these conditions and after the enzyme has remained in the $E_1 \sim P$ conformation for 60 s or longer.

Lipid chain packing as a function of temperature

Examination of the one-dimensional integrated equatorial diffraction patterns $I(r^*, z^* = 0)$ shown in Fig. 2, indicates that initially the equatorial diffraction for temperatures above 10°C consists only of a broad, symmetric peak corresponding to a mean Bragg spacing of $\sim 1/4.5$ $Å^{-1}$. This diffraction originates from melted lipid chains in a highly disordered two-dimensional distribution in the membrane plane, characteristic of a smectic liquid-crystalline state (22). As the temperature is lowered below 10°C an additional sharp peak at a Bragg spacing of $\sim 1/4.2$ $Å^{-1}$ appears, and this peak grows in intensity with decreasing temperature. This diffraction originates from domains of frozen lipid chains ordered in a two-dimensional hexagonal lattice in the membrane plane characteristic of the "gel state" (22). The coexistence of liquid crystalline and gel domains in the membrane is evidence of lipid lateral phase separation (23, 24), which becomes progressively more pronounced as the temperature is lowered further.

As can be seen from the patterns, the first indication of lipid lateral phase separation occurs at a characteristic temperature t_h of ~10°C, which corresponds to the temperature at which the "break" in the plots of the ratio of peak intensities for the third to fourth orders of lamellar diffraction as a function of temperature occurs. The fact that these two temperatures coincide is not surprising, given the fact that lipid is one of the major components of the membrane, and therefore if the structure of the lipids changes, this change will affect the membrane profile structure. In fact, the intensities of the third and fourth orders change in a way that is consistent with what would be expected for a pure lipid bilayer upon occurrence of lipid lateral phase separation (25). However, examination of the membrane profile structure as a function of temperature shows that for temperatures around t_h, the entire membrane profile changes, and not just those regions containing the lipid bilayer. We therefore believe that the correspondence between t_h and the transition temperature derived from the plots of the ratio of peak intensities for the third to fourth orders of the lamellar diffraction really indicates that a structural transition related to the lateral phase separation of the lipids takes place in the entire membrane structure. Comparison with the results previously reported for high $[Mg^{2+}]$ conditions show that in that case there was also a correspondence between the

characteristic temperature t_h for lateral lipid phase separation at 2–3°C and similar changes in the lamellar diffraction. Under high [Mg^{2+}] conditions, the extent of lateral phase separation observed was considerably smaller. A quantitative estimation of the extent of lateral phase separation as a function of temperature, or a more accurate determination of the temperature at which the phase separation begins to appear cannot be easily obtained from our data.

Irreversible lipid phase separation frequently occurs in many biological membrane systems when partial dehydration is used to produce ordered multilayer specimens for x-ray diffraction studies (26). In instances where irreversible phase separation takes place in a membrane system, the lipids generally form a separate phase that is topologically "disconnected" from that in which the protein molecules are located. Evidence to support the interpretation that only reversible lipid lateral phase separation occurred under our experimental conditions comes from the observation that for all samples examined the changes that we observed could be rapidly reversed (in 5–20 min) by reequilibrating the sample at higher temperature.

It is evident from the above that the phase behavior of the membrane lipids is highly dependent on the Mg^{2+} concentration, t_h changing from 2–3°C for [Mg^{2+}] ~ 25 mM to 8–10°C for [Mg^{2+}] ~ 100 μM. The effect of divalent cation concentration on the phase behavior of lipids and lipid mixtures has been studied for lipids with negatively charged polar head groups (27). These studies indicate that increased concentrations of divalent cations tend to increase the amount of lipid lateral phase separation at a given temperature. That observation has been explained by the predictable effects of divalent cations on the otherwise repulsive electrostatic interactions between neighboring polar head groups. Obviously this explanation contradicts our experimental observation of increased phase separation at a given temperature with decreasing [Mg^{2+}]. It has been noted however that the behavior observed greatly depends on the nature of the polar head group (28). Although we are not aware of the existence of any specific study of the influence of divalent cation concentration in the phase separation behavior of biological membranes with lipid composition similar to that of the SR membrane, it has been reported that some glycolipids show a dependence of phase separation behavior on divalent cation concentration similar to that observed by us. At a given temperature, more lipid lateral phase separation was observed when the concentration of Ca^{2+} and/or Mg^{2+} was decreased (29). The behavior of the glycolipid system with respect to lateral phase separation and its dependence on divalent cation concentration was explained on the basis of differences in the degree of hydration of the lipid polar head groups as measured by deuterium NMR experiments. It was proposed that the increased concentration of divalent cations either facilitates the direct hydration of the polar head groups by changing their conformation, or influences their degree of hydration due to the highly hydrated nature of the divalent ions themselves. Increased concentration of divalent cations was therefore expected to produce a metastable, highly hydrated liquid-crystalline phase. It was also pointed out that there are similarities between the physical properties of the studied glycolipids (mono- and diglucosyldiglyceride) and those of phosphatidylethanolamine, a lipid accounting for 21% of the lipid content of the SR membrane (other major components are phosphatidylcholine, another zwitterionic lipid, 65%, and phosphatidylinositol, 9% [30]). Although these studies were performed in a significantly different system they offer a plausible explanation for the SR lipid phase behavior observed in our experiments. This explanation is also consistent with the observed tendency of lipid-water systems to form non–liquid-crystalline phases under low-water-content conditions (22).

Membrane electron density profiles as a function of temperature for low [Mg^{2+}]

The electron density profile of the multilayer unit cell (containing two apposed SR membrane profiles) under low [Mg^{2+}] conditions differs significantly from that observed at high [Mg^{2+}]. This observation applies to all the temperatures examined. One important factor behind the observed differences is a change in the phase of the first order of the lamellar diffraction (see Table 1). In the high [Mg^{2+}] case, the first order changes phase as the temperature is lowered through t_h (2–3°C) and the membrane-pair profile thereby undergoes a structural transition. At low [Mg^{2+}], the phase of the first lamellar diffraction order does not change upon lowering the temperature through the upper characteristic temperature for lipid lateral phase separation t_h, and even at temperatures well above t_h the membrane-pair profile structure is very different from the high [Mg^{2+}], high-temperature profile structure. The box refinement analysis used to verify the phases assigned to the first four lamellar diffraction orders by the GFSDM method does not make any assumptions about the symmetry of the multilayer profile unit cell, and therefore the phases are allowed to take any permissible value between 0 and 2π. This box refinement technique was used in two different ways to check the GFSDM results. First, a low-resolution, box refinement analysis was done using an initial "trial profile function" and the final phases assigned to the first two regions of constant phase (orders 1 and 2, 3, 4) were examined. Roughly opposite phases (0

and π, respectively) were assigned by the box refinement analysis to these two regions, in agreement with the results obtained from the GFSDM analysis. To further check the phases assigned, the box refinement program was given an initial "trial phase function" instead of a "trial profile function" and the way in which the trial phase function was modified as the method iteratively reduced the calculated electron density to zero outside the physical extent of the unit cell profile was examined. If the box refinement algorithm was given a trial phase function that varied linearly over the range covered by the first two constant phase regions, the method introduced a discontinuity such as to make these two regions have nearly opposite phases (again 0 and π, respectively). This is illustrated in Fig. 6 *a*. If, on the other hand, the method was given a trial phase function with nearly opposite phases for the first two constant phase regions, in the iterative process of finding a structure that satisfied the box constraint the method made the phase change between the two regions even more pronounced. This is illustrated in Fig. 6 *b*. The results of the GFSDM analysis, direct application of the box refinement method, as well as the behavior illustrated in Fig. 6 are all conclusive evidence that in fact the phase combinations assigned to the first four orders of lamellar diffraction, and therefore the profile structures of the SR membrane pair are indeed correct and significantly different, for all temperatures studied, under low and high [Mg^{2+}] conditions.

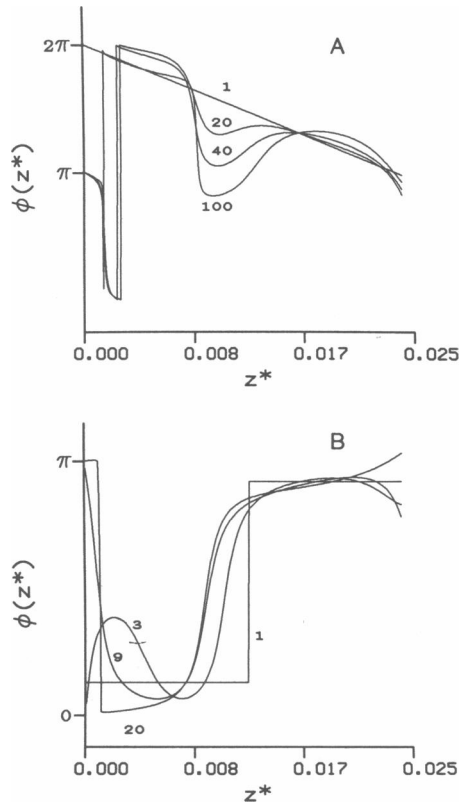

FIGURE 6 Phases predicted by the box refinement method of analysis for the first two constant phase regions of reciprocal space, namely $0.00 \leq z^* \leq 0.01$, and $0.01 \leq z^* \leq 0.03$. Numbers next to the curves indicate the iteration number. Note that more iterations were required for the trial phase function employed in (*A*) because that trial function differed more significantly from the final phases determined by the analysis. These results were used to confirm the phases predicted by the GFSDM analysis. See text for details.

It is important to thoroughly establish the overall origin of the temperature-induced changes observed in the lamellar diffraction. The GFSDM analysis employs least squares fits between the calculated and experimental lamellar intensity functions, between their respective Fourier transforms, and between the calculated and experimental multilayer profile autocorrelation functions (17). The membrane profile itself, the separation of the apposed membrane profiles within the multilayer unit cell, the multilayer lattice disorder parameter, and the lattice periodicity are all free parameters of the analysis. It was found that all of the above parameters necessarily varied with temperature, thereby achieving the best overall fits between the calculated and experimental functions. Variation of any single parameter, while artificially maintaining the value of the remaining ones constant, failed to establish any single parameter as being the dominant factor behind the temperature-induced changes. At the lower temperatures, comparison of the experimental and calculated functions suggested that the GFSDM analysis was overestimating the multilayer lattice disorder. Careful inspection of the experimental lamellar intensity functions $I_c(r^* = 0, z^*)$ indicated that the sharp maxima present in the patterns looked like sharp features superimposed on a broader underlying intensity function whose shape resembled that of $|F_{uc}(z^*)|^2$, the structure factor modulus squared for the membrane-pair profile. It thus appeared that most of the diffracted intensity at lower temperatures arose from an oriented, highly disordered array of flattened membrane pairs, and that the sharp peaks superimposed on this unsampled diffraction arose from a small fraction of the multilayer that was similarly oriented, but much better ordered. The relative contribution of these two fractions was roughly quantified by expressing the experimental lamellar intensity as the sum of unsampled intensity arising from unit cell profiles with little correlation, and sampled intensity coming from a highly ordered portion of the sample, namely:

$$I_c(r^* = 0, z^*) = A|F_{uc}(z^*)|^2 + B|F_{uc}(z^*)|^2 \cdot Z(z^*),$$

where $A + B = 1$, and $Z)(z^*)$ is the interference function for the multilayer lattice. This analysis demonstrated that

the fraction of membrane pairs that was highly ordered was <10% of the total number of diffracting unit cells in the multilayer sample. The presence of this small fraction of better ordered membrane pairs does not affect the final membrane-pair electronic-density profiles obtained from the GFSDM analysis, because $I_c(r^* = 0, z^*)$ still arises almost exclusively from identical membrane-pair profiles. We therefore conclude that the temperature-induced changes in $I_c(r^* = 0, z^*)$ are the combined result of changes in the periodicity of the multilayer lattice, the degree of multilayer lattice disorder, variations in the inter-membrane spacing within the unit cell, and of changes in the profile structure of the SR membrane itself.

Modeling the membrane electron density profiles

To facilitate the interpretation of the continuous unit cell electron density profiles obtained from the GFSDM analysis in terms of molecular components of the SR membrane, a set of typical continuous electron density profiles (see last section of Results) were fit with step-function models. The basic criteria used in building the electron density models were the following. The minimum number of steps required to adequately model the continuous unit cell profile, namely 11 steps for each half of the symmetric unit cell, was used. All steps in the models were assigned a width of 10–12 Å, consistent with the limited spatial resolution (13 Å) to which the continuous unit cell profiles were calculated. The widths of the different steps were necessarily varied, but only within this narrow range, to reproduce distances between important features in the continuous electron density profiles, thereby allowing for small variations with temperature in the width of the intermembrane water space in the unit cell and in the separation between lipid polar head groups across the bilayer profile. The use of step models makes it easier to correlate the temperature-induced changes in the unit cell continuous electron density profiles with changes undergone by particular membrane molecular components, as already demonstrated in the study of the temperature dependence of the unit cell electron density profiles under high $[Mg^{2+}]$ conditions (5). This interpretation is possible because the most significant features in the membrane electron density profiles have been uniquely identified in previous experiments (20). The steps assigned to the 15°C, 100 μM $[Mg^{2+}]$ unit cell profile, as well as their correspondence with molecular components of the SR membrane are shown in Fig. 7.

Fitting of the step models to the calculated continuous electron density profiles was simplified by the fact that only small variations in the width of selected steps were allowed. To optimize the magnitude and width of each

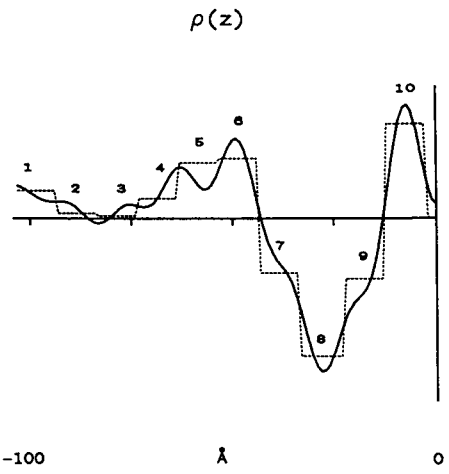

FIGURE 7 Step-function electron density model for the SR membrane profile for T ≃ 15°C and $[Mg^{2+}]$ ≃ 100 μM. Five steps (1–5) are assigned to the membrane extravesicular surface region extending from beyond the lipid polar head groups facing the extravesicular space to the edge of the unit cell. Step 6 represents the lipid polar head groups facing the extravesicular space. Three steps (7–9) are fitted to the hydrocarbon core of the lipid bilayer. Step 10 corresponds to the lipid polar head groups facing the intravesicular space, and step 11 (not numbered in the figure) is a narrow strip that corresponds to the intravesicular water space between the apposed membranes that form the unit cell.

step in the model, a "real space refinement" was carried out. The electron density profile represented by the step model was Fourier transformed, truncated in z^* to match the truncation in the experimental data, and then back-transformed to obtain the continuous electron density profile corresponding to the original step model. Finally, the continuous electron density profile and its autocorrelation function obtained from the model were compared with the corresponding functions obtained from the GFSDM analysis of the experimental data. As indicated before (see last section of Results), the reproducibility of our results for different samples was very high, and therefore, most of the uncertainty in our model calculations comes from the modeling procedure itself, and not from sample-to-sample variability. In carrying out the "real space refinement" described above, the height of the different electron density steps in the model profile was changed by progressively smaller amounts. Variations in the height of the steps in the last iteration were between 2 and 5% of the total height of the step for most steps, particularly those with a large relative electron density. In the case of steps with a small relative electron density, larger variations occurred (in some cases as large as 15%). This is simply a consequence of the fact that variations in the height of steps of small relative electron density do not have a significant effect on the corresponding continuous relative electron density profile and its

autocorrelation function calculated via the real space refinement procedure.

The final autocorrelation function and electron density profile for the best step-function model obtained via such refinement, as well as the corresponding functions obtained from the GFSDM analysis are shown, for the 15°C case, in Fig. 8. Comparable fits were obtained for the other temperatures studied.

It seemed appropriate to analyze the results obtained from the step electron density model calculations by (*a*) studying the changes in the SR membrane profile induced by decreasing the temperature at low (100 μM) [Mg^{2+}] and comparing such changes with those observed under similar circumstances at high (25 mM) [Mg^{2+}], and by (*b*) comparing the profile structure of the membrane for high and low Mg^{2+} concentrations at equivalent, constant temperatures.

The final step-function models for the SR membrane profile (100 μM Mg^{2+}) at 15 and 3°C are shown in Fig. 9. As can be seen from the figure, the most significant changes induced by decreasing the temperature are an increase in electron density in the methylene chain region of the inner monolayer (step 9), and a displacement of protein mass at the extravesicular membrane surface (steps 1–5) in such way that the protein's headpiece is compressed toward its center, creating a "gap" (step 5) between the extravesicular surface lipid polar head groups (step 6) and the region to which protein mass is relocated (step 4).

To compare the changes induced by temperature at low [Mg^{2+}] with those observed at high [Mg^{2+}], the present low [Mg^{2+}] results were analyzed at the same lower resolution (16 Å) at which the system had been previously studied for higher [Mg^{2+}]. Analysis of the low [Mg^{2+}] data at 16 Å resolution indicates, as expected, that the temperature-induced changes in the profile are still of the same nature, although not as well defined as the ones observed in the higher resolution analysis. In Fig. 10, the final step-function models for the SR membrane profile

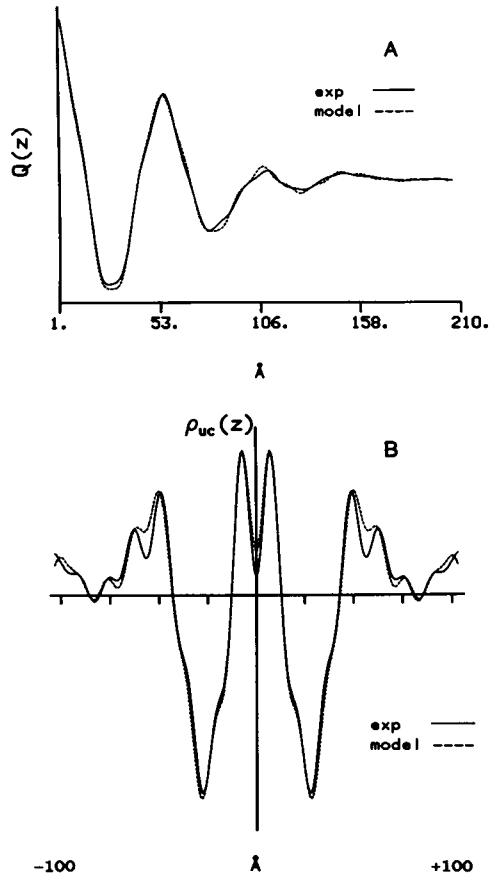

FIGURE 8 Final autocorrelation functions (*A*) and continuous electron density profiles (*B*) obtained from the real space refinement of the step-function electron density models (---) compared with the corresponding functions obtained from the GFSDM analysis (——). The minimum number of steps needed to adequately model the SR membrane profile for [Mg^{2+}] ≃ 100 μM was 11. The width of the steps was kept constant except for small variations (±1 Å) that reflect changes in the width of the lipid bilayer and the intravesicular water space with temperature.

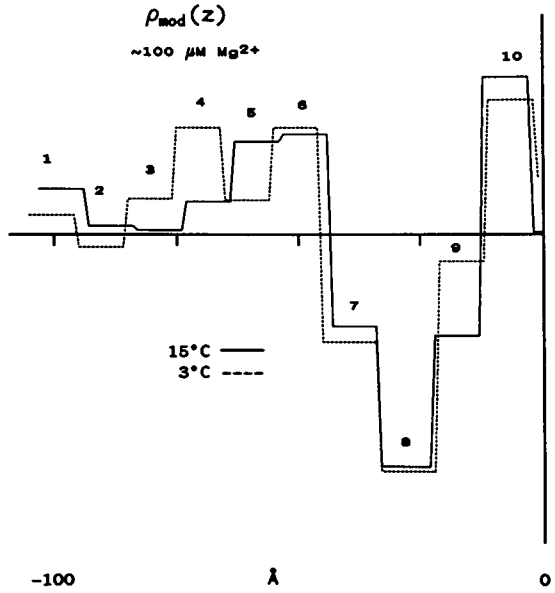

FIGURE 9 Final step-function electron density models of the SR membrane profile (22 steps for the unit cell, corresponding to ~13 Å resolution) for ~100 μM [Mg^{2+}] at 15°C (——) and 3°C (---). Note that the most significant changes occur in the methylene chain region of the inner monolayer (step 9), where the electron density increases with decreasing temperature, and in the region of the membrane outside the lipid bilayer (steps 1–5), i.e., in the headpiece of the Ca^{2+}ATPase. The changes predicted by the calculation conserve the total mass to within 3%. See text for a more detailed discussion of the observed changes.

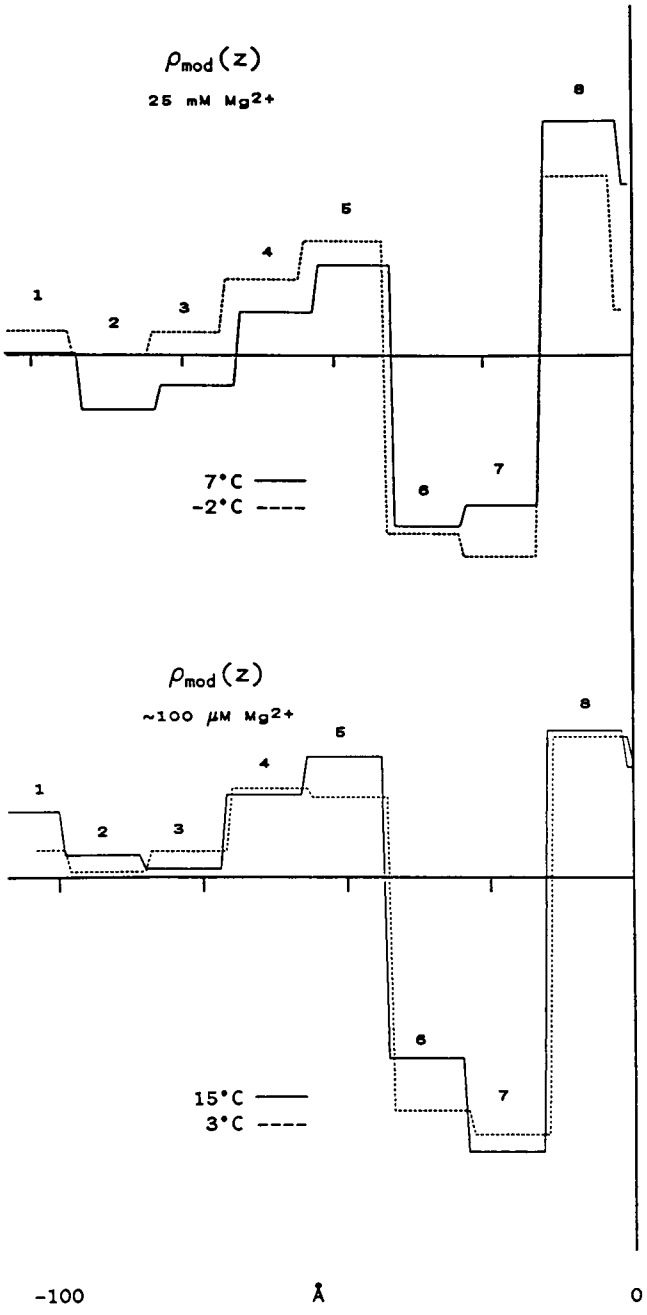

FIGURE 10 Final step-function electron density models of the SR membrane profile (18 steps for the unit cell, corresponding to ~16 Å resolution) for 25 mM [Mg^{2+}] at 7°C (——) and −2°C (----) (from reference 5), and for ~100 μM [Mg^{2+}] at 15°C (——) and 3°C (----). Note that both the initial profiles and the temperature-induced changes in the profile are different in both cases. Modeling of the low [Mg^{2+}] profiles improved significantly when the number of steps was increased, and this was taken as a further manifestation of the existence of basic differences between the low and high [Mg^{2+}] profiles. Note that, due to the lesser number of steps used in this lower resolution model, numbers assigned to steps corresponding to the same regions of the membrane profiles are different in Figs. 9 and 10.

for 25 mM [Mg^{2+}] at 7 and −2°C (5), as well as the corresponding results for 100 μM [Mg^{2+}] at 15 and 3°C, are shown. Notice that, because a smaller number of steps were used to model the membrane electron density profile at this lower resolution, steps corresponding to the same regions of the membrane are numbered differently in Figs. 9 and 10. A decrease of temperature under high [Mg^{2+}] conditions causes a loss of electron density in the inner monolayer (step 7). That density is more or less uniformly redistributed over the region of the membrane including the extravesicular lipid polar head groups (step 5), and the region outside the lipid bilayer (steps 1–4). For low [Mg^{2+}], a similar change in temperature causes a gain of electron density in the inner monolayer (step 7), and even when movement of mass out of the lipid bilayer region of the membrane is also observed, the way in which mass is redistributed is different. Therefore, the changes induced by decreasing the temperature at the two [Mg^{2+}] studied are definitively distinct. Furthermore, the high-temperature (15°C), low-[Mg^{2+}] profile is more similar to (but still different from) the low-temperature (−2°C), high-[Mg^{2+}] profile than to the high-temperature (7°C), high-[Mg^{2+}] one.

To best determine the temperature-independent effect of [Mg^{2+}] on the SR membrane profile structure, patterns corresponding to different magnesium concentrations and equivalent temperatures have to be compared. The occurrence of lipid lateral phase separation affects the membrane profile structure, and because the upper characteristic temperature for lateral phase separation of the membrane lipids, t_h, depends strongly on the [Mg^{2+}], it seemed reasonable to compare profiles corresponding to the same reduced temperatures referenced to the value of t_h for the corresponding [Mg^{2+}]. Continuous electron density profiles and their best step-function models for the SR membrane for two different Mg^{2+} concentrations (~25 mM and ~100 μM) and roughly equivalent temperatures (referenced to ~2 and ~9°C, the values of t_h that correspond to the respective [Mg^{2+}]) are shown in Fig. 11. As mentioned before, the phases assigned to the first lamellar Bragg order in each case are opposite, and for the higher [Mg^{2+}] this phase changes when the temperature is lowered beyond t_h (5). This fact partially explains the large differences between the two profiles. Note that at the lower [Mg^{2+}] the separation between the lipid polar head groups (steps 6 and 10) is larger and the structure of the lipid hydrocarbon core region is different. For the higher [Mg^{2+}], two steps (6 and 7) are sufficient to adequately model the hydrocarbon core region. The low [Mg^{2+}] profile cannot be adequately modeled assigning only two steps to the hydrocarbon core region. The structure of this part of the membrane is sufficiently different that three electron density steps (7–9) are required to model it appropriately.

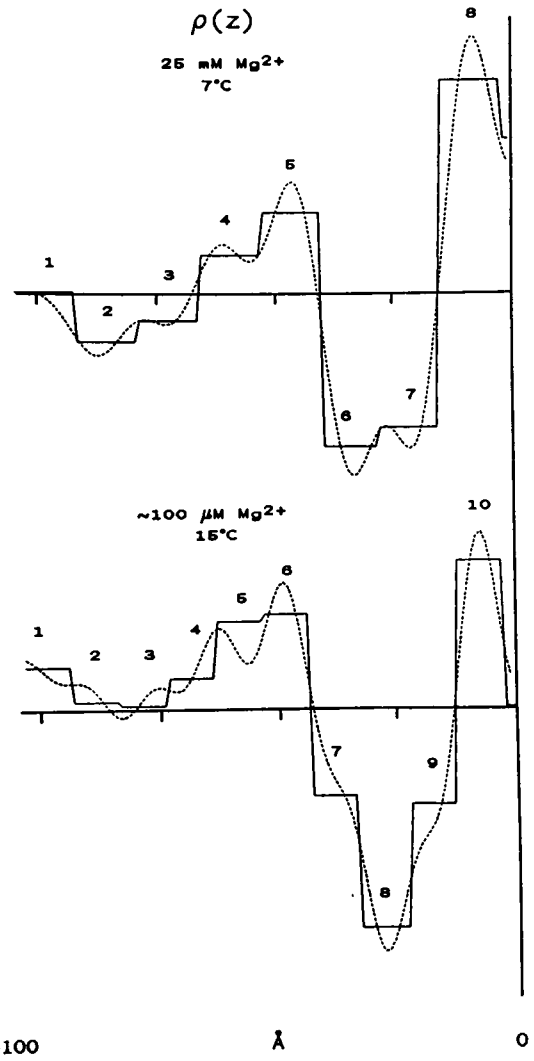

FIGURE 11 Continuous electron density profiles and their step-function electron density models of the SR membrane for two different $[Mg^{2+}]$ (~25 mM and ~100 μM) and roughly equivalent temperatures (referenced to ~2° and ~9°C, the values of t_h that correspond to the respective $[Mg^{2+}]$). The phases assigned to the first lamellar Bragg order in each case are opposite. At the higher $[Mg^{2+}]$ this phase changes when the temperature is lowered beyond t_h, and that partially explains the large differences between the two profiles. Note that at the lower $[Mg^{2+}]$ the separation between the polar head groups is larger, and the structure of the lipid hydrocarbon core region different enough that three electron density steps are needed to adequately model it, as opposed to only two steps for the higher $[Mg^{2+}]$. Also note that protein mass has moved the space outside the lipid bilayer on the extravesicular membrane surface, a general change also observed to occur with decreasing temperature independently of the $[Mg^{2+}]$.

The changes in the hydrocarbon core region of the membrane profile induced by decreasing temperature or decreasing $[Mg^{2+}]$ are completely consistent with what one would expect from the changes observed in the equatorial diffraction. The occurrence of lipid lateral phase separation is indicated, in the equatorial diffraction patterns, by the appearence of a sharp reflection corresponding to a Bragg spacing of 1/4.2 $Å^{-1}$. This sharp reflection at larger r^* arises because the frozen lipid fatty-acid chains involved in lateral phase separation are packed more tightly in the membrane plane. In the membrane electron density profile, this phenomenon causes an increase in the average lipid polar headgroup separation across the bilayer profile, an increase in the average electron density in the region of the profile corresponding to the lipid fatty-acid chain methylene groups, and correspondingly, it also makes the average position in the bilayer profile of the low-electron-density trough corresponding to the terminal methyl groups of the lipid chains to be much better defined (22, 31). The fact that the low-$[Mg^{2+}]$ profiles can be better modeled using three (instead of two) steps for the hydrocarbon core region of the membrane is a manifestation of the fact that the positional distribution of the terminal methyl groups of the lipid fatty-acid chains in the membrane profile is much narrower under these conditions, as a direct consequence of the presence of more frozen lipid chains in a "gel state." All these considerations lead us to believe that the increase in electron density in the inner monolayer (step 9 in Fig. 9) of the SR membrane observed under low-$[Mg^{2+}]$ conditions when the temperature is decreased, is most likely due to the preferential occurrence of lateral phase separation in that monolayer, and not to an increase in the distribution of protein mass into that region of the membrane profile.

Structure-function correlations

It is interesting to note that in the low-$[Mg^{2+}]$ profile, more protein mass has moved to the extravesicular surface of the membrane (steps 1–5), a general change that is also observed to occur with decreasing temperature independently of the $[Mg^{2+}]$. Thus, a decrease in temperature and/or $[Mg^{2+}]$ will cause changes in the structure of the membrane that result in movement of protein mass out of the lipid bilayer and onto the extravesicular surface of the membrane. This is opposite to the changes that have been observed upon formation of the E_1~P intermediate. At high $[Mg^{2+}]$ (25 mM) and temperatures between −2 and 7°C (32, 33), phosphorylation of the Ca^{2+}ATPase (via flash-photolysis of caged ATP) and formation of the E_1~P intermediate result in a net movement of protein mass from the extravesicular surface into the lipid bilayer of the membrane. Because decreasing temperature or decreasing $[Mg^{2+}]$ cause the structure of the Ca^{2+}ATPase to become increasingly different from the structure of the E_1~P intermediate, both factors should cause an increase in the activation energy for formation of E_1~P, and should therefore affect the kinet-

ics of the fast phase of Ca^{2+} uptake, associated with $E_1{\sim}P$ formation. Indeed, the results reported here indicate that the fast phase of Ca^{2+} uptake is greatly slowed down by decreasing $[Mg^{2+}]$, and previous results from our laboratory (9) indicate that at constant $[Mg^{2+}]$ (25 mM) decreasing temperature also slows down the fast phase.

Temperature and $[Mg^{2+}]$ not only affect the formation of $E_1{\sim}P$, they also have a very significant effect on the lifetime of this intermediate. We are inclined to believe that the effect of temperature and $[Mg^{2+}]$ on the lifetime of $E_1{\sim}P$ has also a structural origin. We have already reported that at high $[Mg^{2+}]$ (25 mM), significant differences between the structures of $E_1{\sim}P$ at -2 and 7°C provide one of two possible explanations for the time-resolved x-ray diffraction data (32, 33).

CONCLUSION

The results from our studies indicate that the profile structure of the SR membrane, the lateral phase separation behavior of the membrane lipids, and the kinetics of Ca^{2+} uptake (in particular the formation and lifetime of the $E_1{\sim}P$ intermediate) are all dependent on the temperature and the $[Mg^{2+}]$. Furthermore, some interesting interdependences between the above characteristics of the SR membrane were observed.

At constant $[Mg^{2+}]$, variations in temperature produce changes in the membrane profile structure and in the kinetics of Ca^{2+} uptake. Under the experimental conditions in our study, these changes seem to be correlated with the value of the upper characteristic temperature of lipid lateral phase separation in the membrane, t_h. Our results therefore indicate that structural changes affect the kinetics of Ca^{2+} uptake by the SR and that changes in the structure and function of the SR membrane could be modulated by changes in the structure of the membrane lipids.

On the other hand, at constant reduced temperatures (referenced to the appropriate value of t_h), changes in $[Mg^{2+}]$ will produce significant changes in the SR membrane profile structure and in the kinetics of Ca^{2+} uptake. This holds true even for temperatures well above the value of t_h for the $[Mg^{2+}]$ considered. It is therefore possible that $[Mg^{2+}]$ has a direct effect on the structure of the Ca^{2+}ATPase and is thereby capable of affecting its function without changing so significantly the structure of the membrane lipids.

It is important to investigate whether induced changes in lipid structure are responsible for affecting the structure of the Ca^{2+}ATPase, or whether induced changes in the structure of the protein are responsible for affecting the structure of the lipids, which are manifest under our experimental conditions by lateral phase separation when the temperature is decreased. We have made a preliminary report (34) of our investigation of the lateral phase separation behavior of lipids isolated from the SR membrane, and of the effect of water activity on the phase diagram of both the membrane and its isolated lipids. Our results indicate that indeed, the behavior of the lipids is the driving force behind the Mg^{2+}-sensitive, temperature-induced structural transition observed for the Ca^{2+}ATPase. A full account of these results is in preparation.

This work was supported by National Institute of Health grant HL-18708 to J. K. Blasie.

Received for publication 16 May 1988 and in final form 12 December 1988.

REFERENCES

1. Dupont, Y. 1980. Occlusion of divalent cations in the phosphorylated calcium pump of sarcoplasmic reticulum. *Eur. J. Biochem.* 109:231–238.
2. Shigekawa, M., S. Wakabayashi, and H. Nakamura. 1983. Reaction mechanism of Ca^{2+}-dependent adenosine triphosphatase of sarcoplasmic reticulum. *J. Biol. Chem.* 258:8698–8707.
3. Domonkos, J., L. Heiner, and M. Vargha, Jr. 1985. The effect of di- and trivalent cations on the phosphorylation of the Ca^{2+}-ATPase in sarcoplasmic reticulum vesicles. *Biochim. Biophys. Acta.* 817:1–6.
4. Shigekawa, M., S. Wakabayashi, and H. Nakamura. 1983. Effect of divalent cation bound to the ATPase of sarcoplasmic reticulum. *J. Biol. Chem.* 258:14157–14161.
5. Pascolini, D., and J. K. Blasie. 1988. Moderate resolution profile structure of the sarcoplasmic reticulum membrane under "low" temperature conditions for the transient trapping of $E_1{\sim}P$. *Biophys. J.* 54:669–678.
6. deMeis, L., and A. L. Viana. 1979. Energy interconversion by the Ca^{2+}-dependent ATPase of the sarcoplasmic reticulum. *Annu. Rev. Biochem.* 48:275–292.
7. Yamada, S., J. Fujii, and H. Katayama. 1986. Sarcoplasmic reticulum Ca-ATPase: distinction of phosphoenzymes formed from MgATP and CaATP as substrates and interconversion of the phosphoenzymes by Mg^{2+} and Ca^{2+}. *J. Biochem.* 100:1329–1342.
8. Meissner, G., G. E. Conner, and S. Fleischer. 1973. Isolation of sarcoplasmic reticulum by zonal centrifugation and purification of Ca^{2+}-pump and Ca^{2+}-binding proteins. *Biochim. Biophys. Acta.* 298:246–269.
9. Pierce, D., A. Scarpa, M. Topp, and J. K. Blasie. 1983. Kinetics of calcium uptake by isolated sarcoplasmic reticulum vesicles using flash photolysis of caged adenosine 5'-triphosphate. *Biochemistry.* 22:5254–5261.
10. Pierce, D., A. Scarpa, D. Trentham, M. Topp and J. K. Blasie. 1983. Comparison of the kinetics of calcium transport in vesicular dispersions and oriented multilayers of isolated sarcoplasmic reticulum membranes. *Biophys. J.* 44:365–373.
11. Herbette, L., A. Marquardt, A. Scarpa, and J. K. Blasie. 1977. A

direct analysis of lamellar x-ray diffraction from hydrated oriented multilayers of fully functional sarcoplasmic reticulum. *Biophys. J.* 20:245–272.

12. Franks, A. 1955. An optically focusing x-ray diffraction camera. *Proc. Phys. Soc. B.* 68:1054–1064.
13. Warren, B. E. 1969. X-Ray diffraction. Addison-Wesley Publishing Co., Reading, MA. 381 pp.
14. McFarland, B. H., and G. Inessi. 1971. Solubilization of sarcoplasmic reticulum with Triton X-100. *Arch. Biochem. Biophys.* 145:456–464.
15. Pierce, D. H. 1982. Kinetics of calcium uptake by the sarcoplasmic reticulum membrane. Ph.D. dissertation. University of Pennsylvania, Philadelphia, Pa.
16. Henderson, R. 1975. The structure of the purple membrane from Halobacterium halobium: analysis of the x-ray diffraction pattern. *J. Mol. Biol.* 93:123–138.
17. Schwartz, S., J. Cain, E. Dratz, and J. K. Blasie. 1975. An analysis of lamellar x-ray diffraction from disordered membrane multilayers with application to data from retinal rod outer segment. *Biophys. J.* 15:1201–1233.
18. Stroud, R. M., and D. A. Agard. 1979. Structure determination of assymetric membrane profiles using an iterative Fourier method. *Biophys. J.* 25:495–512.
19. Weaver, H. J. 1983. Applications of Discrete and Continous Fourier Analysis. John Wiley & Sons, New York. 375 pp.
20. Herbette, L., P. DeFoor, S. Fleischer, D. Pascolini, A. Scarpa, and J. K. Blasie. 1985. The separate profile structures of the functional calcium pump protein and the phospholipid bilayer within isolated sarcoplasmic reticulum membranes determined by x-ray and neutron diffraction. *Biochim. Biophys. Acta.* 817:103–122.
21. Takakuwa, Y., and T. Kanazawa. 1979. Slow transition of phosphoenzyme from ADP-sensitive to ADP-insensitive forms in solubilized Ca^{2+}, Mg^{2+}-ATPase of sarcoplasmic reticulum: evidence for retarded dissociation of Ca^{2+} from the phosphoenzyme. *Biochem. Biophys. Res. Commun.* 88:1209–1216.
22. Luzzati, V., and A. Tardieu. 1974. Lipid phases: structure and structural transitions. *Annu. Rev. Phys. Chem.* 25:79–94.
23. Shimshick, E., and H. M. McConnell. 1973. Lateral phase separation in phospholipid membranes. *Biochemistry.* 12:2351–2360.
24. Kleemann, W., and H. M. McConnell. 1974. Lateral phase separation in *E. coli* membranes. *Biochim. Biophys. Acta.* 345:220–230.
25. Wilkins, M. H. F., A. E. Blaurock, and D. M. Engelman. 1971. Bilayer structure in membranes. *Nature (Lond.).* 230:72–76.
26. Gruner, S. M., K. J. Rothschild, and N. A. Clark. 1982. X-Ray diffraction and electron microscopy study of phase separation in retinal rod outer segment photoreceptor membrane multilayers. *Biophys. J.* 39:241–251.
27. Düzgünes, N. 1985. Membrane fusion. *Subcell. Biochem.* 11:195–287.
28. Van Dijck, M., B. De Kruijff, A. Verkleij, L. Van Deenen, and U. de Gier. 1978. Comparative studies on the effects of pH and Ca^{2+} on layers of various negatively charged phospholipids to their mixtures with phosphatidylcholine. *Biochim. Biophys. Acta.* 512:84–96.
29. Wieslander, A., J. Ulmius, G. Lindblom, and K. Fontel. 1978. Water binding and phase structures for different *Acholeplasma laidlawii* membrane lipids studied by deuteron nuclear magnetic resonance and x-ray diffraction. *Biochim. Biophys. Acta.* 512:241–253.
30. Hidalgo, C., N. Ikemoto, and J. Gergely. 1976. Role of phospholipids in the calcium-dependent ATPase of the sarcoplasmic reticulum. *J. Biol. Chem.* 251:4224–4232.
31. Levine, Y. K., and M. H. F. Wilkins. 1971. Structure of oriented lipid bilayers. *Nature (Lond.).* 230:69–72.
32. Blasie, J. K., L. Herbette, D. Pascolini, V. Skita, D. H. Pierce, and A. Scarpa. 1985. Time-resolved x-ray diffraction studies of the sarcoplasmic reticulum membrane during active transport. *Biophys. J.* 48:9–18.
33. Pascolini, D., L. Herbette, V. Skita, F. Asturias, A. Scarpa, and J. K. Blasie. 1988. Changes in the sarcoplasmic reticulum membrane profile induced by enzyme phosphorylation to E_1~P at 16 Å resolution via time resolved x-ray diffraction. *Biophys. J.* 54:679–688.
34. Asturias, F., D. Pascolini, and J. K. Blasie. 1989. Effect of lipid lateral phase separation on the Ca^{2+} ATPase of the sarcoplasmic reticulum. *Biophys. J.* 55:98a.